



Floating double boost converter

Felix A. Himmelstoss * 

University of Applied Sciences Technikum Wien, Faculty of Electronic Engineering and Entrepreneurship, Vienna, Austria, felix.himmelstoss@technikum-wien.at

Helmut L. Votzi 

University of Applied Sciences Technikum Wien, Faculty of Electronic Engineering and Entrepreneurship, Vienna, Austria, helmut.votzi@technikum-wien.at

Submitted: 30.07.2024

Accepted: 06.02.2025

Published: 31.03.2025



* Corresponding Author

Abstract: The combination of two converters to a dual floating converter is an interesting concept. Here a positive output double floating boost converter is treated. The concept is explained step by step with the help of signal drawings and basic calculations. The fourth order model is derived for large and small signals, idealized components, and can be used to study the converter when it is not built symmetrically. A simpler model of second order is sufficient, when the two converter stages have nearly the same component values. The position of the zeroes and the poles are treated. The turn-on and the soft-start of the converter are also studied. With an additional stage the inrush into the converter can be avoided and the converter can be protected from short-circuit, no load, overheating, and overload. Simulations with the help of LTSpice are presented to validate the considerations. The influence of the parasitic capacitors to ground are studied. Interesting modifications of the converter are shown. Experimental results of a small laboratory converter are presented.

Keywords: Boost converter, DC/DC converter, Inrush, Modelling, Simulation

Cite this paper as: Himmelstoss FA, & Votzi HL, Floating double boost converter. *Journal of Energy Systems* 2025; 9(1): 85-104, DOI: 10.30521/jes.1525077

2025 Published by peer-reviewed open access scientific journal, JES at DergiPark (<https://dergipark.org.tr/jes>)

1. INTRODUCTION

To increase the power of a converter, two equal converter stages can be combined. The advantage is that the power is now divided in two equal parts, making the cooling of the system more easily, because of a better distribution of the losses. Furthermore, the voltage transformation ratio is changed. The floating double boost converter (Fig. 1) consists of two boost converters, each built up by an active switch S , a passive switch D , an inductor L , and a capacitor C . The two Boost converters are connected in parallel at the input and in series at the output. To increase the frequency at the input side, the converters are controlled by control signals which are shifted by 180° . With higher frequency the voltage ripple at the output of the converter is reduced, or when the same ripple is desired the values of the output capacitors can be reduced. The frequency of the input current is also doubled leading to the reduction of the value of an input capacitor.

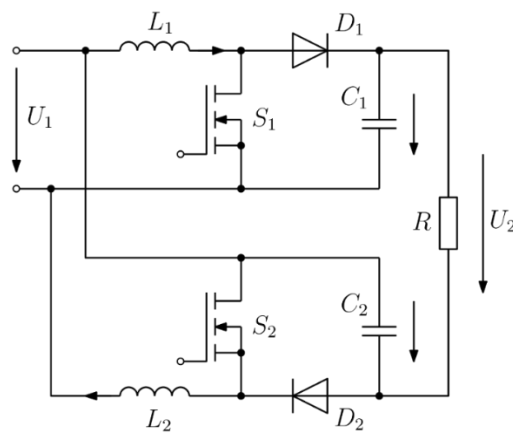


Figure 1. Floating double boost converter (FDBC).

The boost converter and all the other basic converters are comprehensively explained in the textbooks on Power Electronics, e.g. [1,2,3,4] is a comprehensive review of step-up converters. Ref. [5] shows more than hundred topologies for DC/DC converters. A theoretical treatment how to construct DC/DC converters is the paper [6]. All these converters can be enhanced to realize floating two stage converters.

In the literature floating double converters are shown especially for the boost converter. It should be mentioned, however, that this concept can be used also for other converter structures. In Ref. [7], a floating double boost converter is treated which combines two interleaved boost converters, so the converter consists of four converter stages. Ref. [8] shows floating double boost converters, which combine cascaded boost converters. In Ref. [9], triple interleaved boost converters are combined to a dual boost converter. Ref. [10] treats an improved floating interleaved boost converter for photovoltaic systems which uses additional resonant circuits. In Ref. [11], an experimental validation of high-voltage-ratio low input current ripple converters for hybrid fuel cell supercapacitor systems is treated, which uses the basic topology and additional two and three interleaved stages. Ref. [12] studies an extended state observer-based sliding-mode control for floating interleaved boost converters. Ref. [13] uses a bidirectional structure to study an advanced robust noise suppression control for fuel cell electric vehicles. Ref. [14] treats an improved floating interleaved boost converter with low-ripple input current for fuel cell applications. It uses tapped inductors and additional resonance circuits. The controller design and a fault tolerance analysis of a 4-phase floating interleaved Boost converter for fuel cell electric vehicles is treated in Ref. [15]. Ref. [16] shows an experimental evaluation of an interleaved Boost topology, optimized for peak power tracking control in solar application. Ref. [17] applies the model predictive control to the floating interleaved boost converter. Ref. [18] uses the floating Boost

converter as supply to a DC micro-grid. Ref. [19] explains the development of a four phase floating interleaved Boost converter for photovoltaic systems.

A special floating double Buck-Boost converter is an interesting concept as a driver for permanent excited DC machines as treated in Ref. [20]. The floating double converter concept can be also combined with the tristate concept; leading to converters where the active switch is replaced by two electronic switches and an additional diode. This leads to an additional degree of freedom in the voltage transformation ratio and in some cases the zero on the right side of the complex plane in the transfer function is avoided, making the design of the controller easier [21]. The SEPIC converter [22] can also be used as circuit for the floating double stage converter.

One can earth one side of the system, either the input side or the output side, depending on the application and for security reasons. Through these parasitic capacitors to ground of the floating side of the converter, currents flow to ground according to the change of the voltages. The higher the derivative of the voltage, the higher the current. In Sec. 5, this will be treated more in detail. Sec. 2 shows a step by step analysis of the converter with figures of the voltages across and the currents through the components. In section 3 the calculation of the mathematical description of the converter is explained and the complex fourth order model is given. By using nearly similar stages a simpler second order model can be used. After linearization of the nonlinear large system, the small signal model is achieved from which transfer functions can be calculated. Sec. 4 describes the inrush current problem and a simple method to avoid it is given. This extension can be also used as electronic fuse and protect the circuit in the case of short-circuit and open-circuit. (Remember: A boost converter is not open-circuit proved; with no load and a clocking transistor the output voltage increases all the time (until the losses are equal to the energy which is taken from the source during one period, or one of the components brakes through or is destroyed)). In Sec. 6, two modifications of the system are shown. In the modified converter the bulk capacitors of the stages are not connected in parallel to the output terminals, but between the input and the output connectors. This has the advantage that no inrush current occurs when the converter is connected to a stable input voltage source. To reduce the conduction loss of the converters, active switches have to be applied instead of the diodes. With this modification also a two-quadrant operation is possible. Energy can be transferred from the input to output, but also in the other direction from the output side to the input side. The converter can now be used to charge or discharge batteries or double-layer capacitors, e.g., in a micro-grid application. In Sec. 7, some oscilloscope pictures are displayed.

2. STEP BY STEP EXPLANATION

2.1. Graphical Analyses

To get a clear understanding of the converter, we look at the voltages across the components (Figs. 2(a-d)), and start by drawing the voltages across the inductors. The signals are drawn for the steady-state in the continuous inductor current mode and for ideal components. The control signals are shifted by 180 degrees and have a duty cycle of one third. When S1 is turned on, the input voltage U1 is across the first coil L1 and when the switch turns off, the current commutates into the diode D1, and the voltage across the coil is now the input voltage minus the voltage across C1. When the switch S2 is on, U1 is across the coil L2 and when it is off, the difference between input voltage and output voltage is across the inductor L2. The mean value of the voltage across the inductors must be zero. Arbitrarily, we start with an input voltage of two divisions. From these signals all other signals can be drawn. We can now draw the voltages at the capacitors and also the input voltage. From Fig. 1 and with Kirchhoff's voltage law (KVL) one immediately see that the output voltage U2 is equal to the sum of the output voltages of the two Boost converters minus the input voltage. The output voltage must have four divisions. Now we look at the active switches. When the switches are on, no voltage is across them and when the switches are off, the voltage across the respective capacitor stresses the active switches. Next, we look at the passive switches (diodes). When the diodes conduct, the voltage across them is zero and when they are

blocking, that is during the on-time of the active switch, the negative voltage across the capacitor stresses the diode.

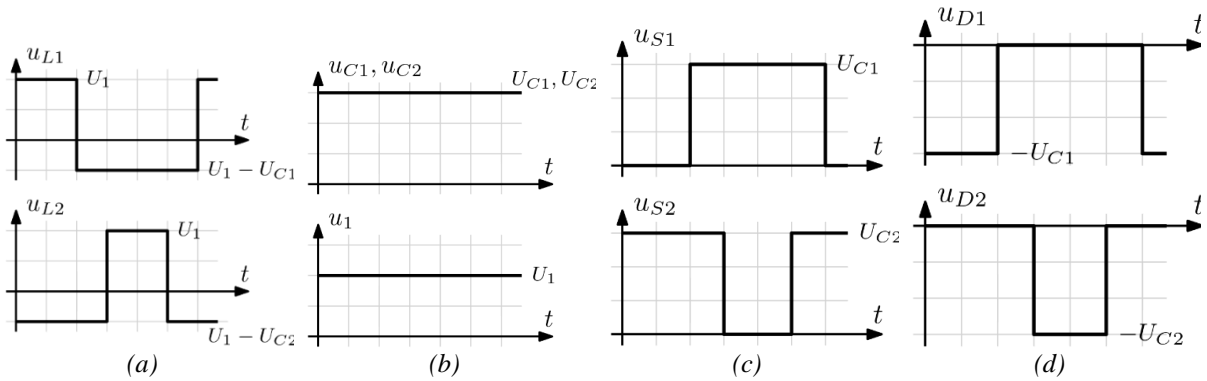


Figure 2. Voltages (a) across the coils, (b) across the capacitors, (c) across the active switches, and (d) across the diodes.

To construct the currents (Fig. 3(a-d)) through the components we use as starting point the load current and choose arbitrarily two divisions. When the active switch of the respective converter part is on, the capacitor has to supply the load. When the active switch is off, the current through the inductor is fed via the diode to the output and the capacitor has to take the surplus of the current. First one draws the mean values of the currents through the inductors (the current through the capacitor must be zero in the mean) and afterward refines it with the ripple of the inductor currents. The current through the coils increases when a positive voltage is across them and decreases, when a negative voltage is across them. Now one can look at the currents through the semiconductors. When the switch or the diode is on, the current through the inductors flows through the semiconductors and when the switch or the diode is blocking, no current flows through them. At last we construct the input current. The frequency of the AC component is double the switching frequency of the converters because of the phase shift between the control signals. The ripple is also reduced.

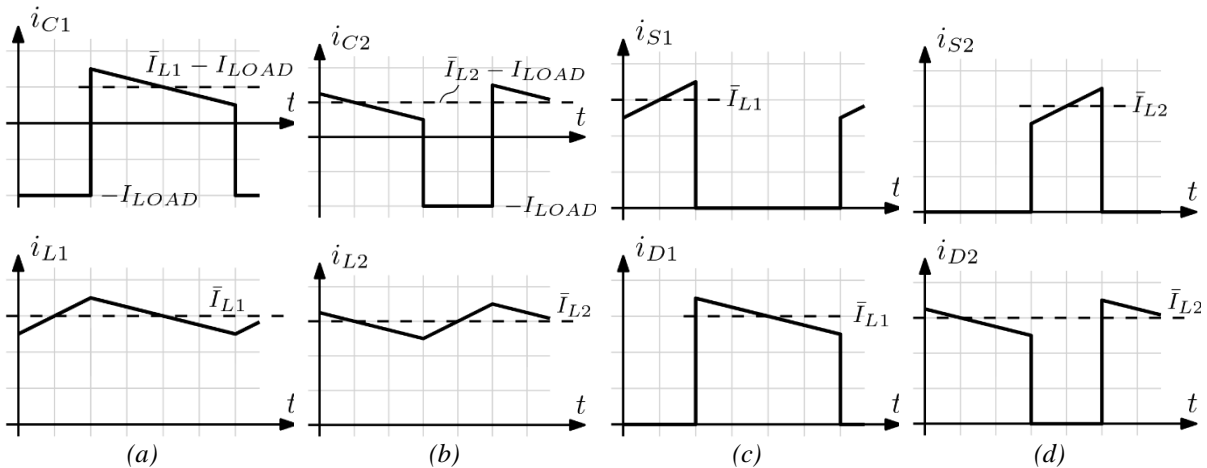


Figure 3. Currents through (a) C1 and L1, (b) C2 and L2, (c) first switch and diode, and (d) second switch and diode.

Fig. 4 shows the input current, the currents through the coils, the load current, the output voltage, the input voltage and the control signals. Figure 5 shows the input current, the current through S1, the current through D1, the current through D2, the current through L2, the current through L1, the load current, the output voltage, the input voltage, the control signal of S1, and the control signal of S2. The parameters for the converter are $L1=L2=47 \mu\text{H}$, $C1=C2=330 \mu\text{F}$, $R=12.5 \Omega$.

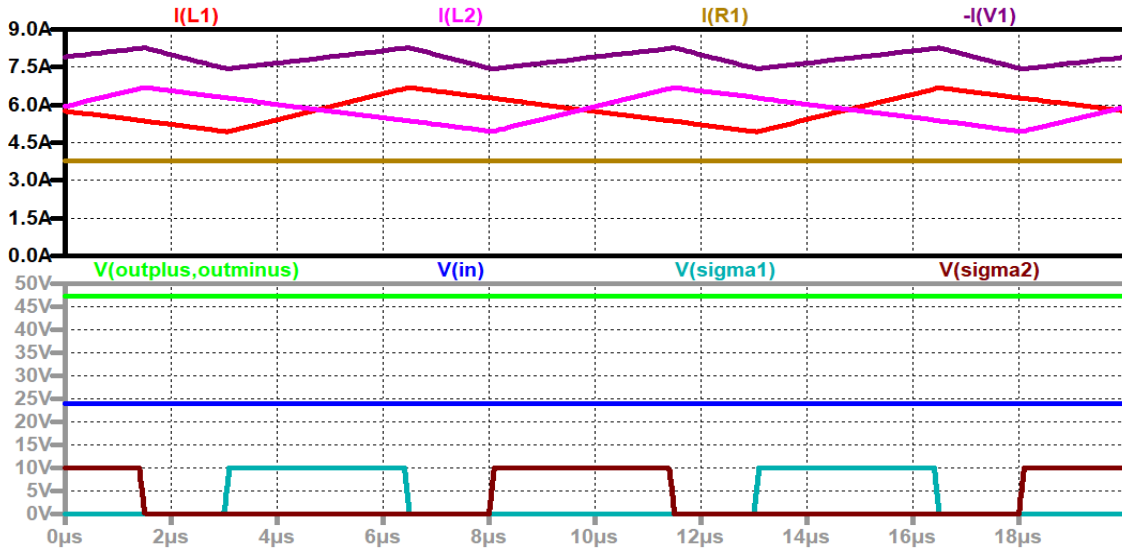


Figure 4. FDBC in steady state up to down: input current (deep violet), current through S1 (dark blue); current through D1 (grey), current through D2 (dark green); current through L2 (violet), current through L1 (red), load current (brown); output voltage (green), input voltage (blue), control signal of S1 (turquoise), control signal of S2 (black).

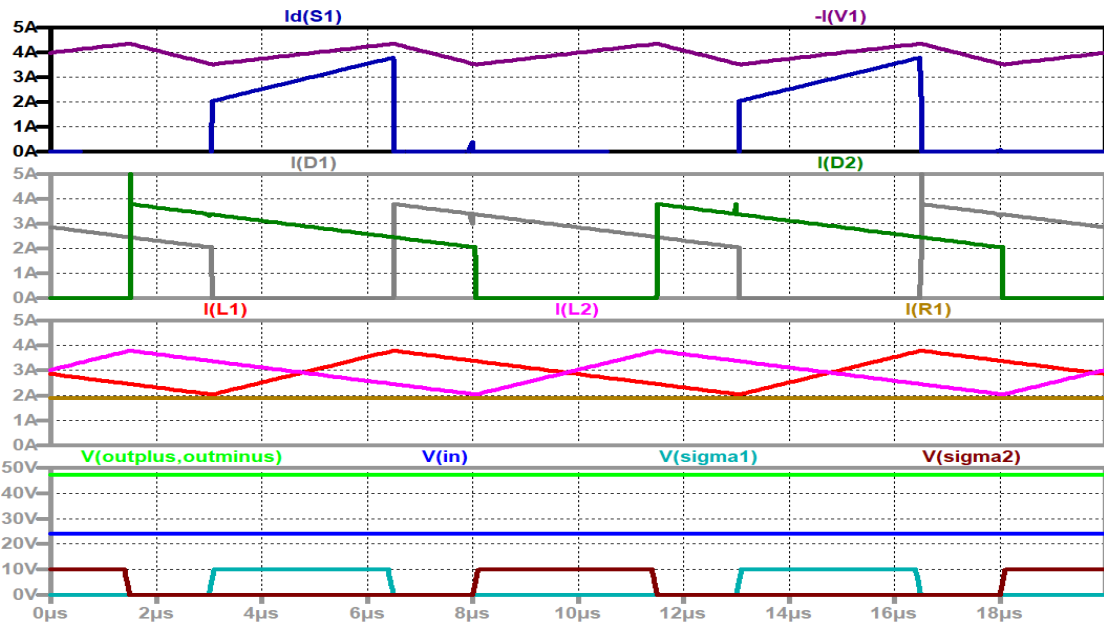


Figure 5. FDBC in steady state up to down with smaller load: input current (deep violet), current through S1 (dark blue); current through D1 (grey), current through D2 (dark green); current through L2 (violet), current through L1 (red), load current (brown); output voltage (green), input voltage (blue), control signal of S1 (turquoise), control signal of S2 (black)

2.2. Basic Calculations

After the graphical analyses of the converter we make some simple calculations. The voltage-time balance of the coils (index i is 1 or 2, naming the converter part) can be written according to,

$$U_1 d_i = |U_1 - U_{Ci}|(1 - d_i) \quad (1)$$

which leads to the voltage across the capacitor C_i ,

$$U_{Ci} = \frac{1}{1-d_i} U_1. \quad (2)$$

The output voltage is,

$$U_2 = U_{C1} - U_1 + U_{C2} = \left(\frac{1}{1-d_1} - 1 + \frac{1}{1-d_2} \right) U_1. \quad (3)$$

When both duty cycles are equal (this is to be preferred because the components are stressed equally), this leads to the voltage transformation ratio

$$M = \frac{U_2}{U_1} = \frac{1+d}{1-d}. \quad (4)$$

To get the connections between the currents one must again look at the currents through the capacitors. The charge balance of the capacitors must be,

$$I_{LOAD} \cdot d_i = (\bar{I}_{Li} - I_{LOAD}) \cdot (1-d_i). \quad (5)$$

Therefore, one gets for the mean value of the inductor current,

$$\bar{I}_{Li} = \frac{I_{LOAD}}{1-d_i}. \quad (6)$$

The mean value of the input current is the mean values of the inductor currents reduced by the load current. For equal duty cycles one gets,

$$\bar{I}_{IN} = 2 \frac{I_{LOAD}}{1-d} - I_{LOAD} = I_{LOAD} \frac{2-1+d}{1-d} = I_{LOAD} \frac{1+d}{1-d} \text{ leading to } \frac{\bar{I}_{IN}}{I_{LOAD}} = \frac{1+d}{1-d}. \quad (7)$$

One can see that the input power is equal to the output power, as it should be with an ideal converter.

3. MODEL OF THE CONVERTER

Both boost converters can be treated separately. In mode M1, the switch is on and the diode is off, and one gets for the change of the currents through the coils

$$\frac{di_{Li}}{dt} = \frac{u_1}{L_i}. \quad (8)$$

The current through the capacitor is equal to the negative load current. The load current can be calculated with Ohm's law to,

$$i_{LOAD} = \frac{u_{C1} + u_{C2} - u_1}{R}. \quad (9)$$

The state equation for the capacitors can therefore be written according to,

$$\frac{du_{Ci}}{dt} = \frac{(-u_{C1} - u_{C2} + u_1)/R}{C_i}. \quad (10)$$

The state equations for the second mode M2 (active switch off, diode on) are,

$$\frac{di_{Li}}{dt} = \frac{u_1 - u_{Ci}}{L_i}, \quad (11)$$

$$\frac{du_{Ci}}{dt} = \frac{i_{Li} - (u_{C1} + u_{C2} - u_1)/R}{C_i}. \quad (12)$$

One can write these four equations into one matrix differential equation for mode M1 and M2,

$$\frac{d}{dt} \begin{pmatrix} i_{L1} \\ i_{L2} \\ u_{C1} \\ u_{C2} \end{pmatrix} = \begin{bmatrix} 0 & 0 & 0 & 0 \\ 0 & 0 & 0 & 0 \\ 0 & 0 & -\frac{1}{RC_1} & -\frac{1}{RC_1} \\ 0 & 0 & -\frac{1}{RC_2} & -\frac{1}{RC_2} \end{bmatrix} \begin{pmatrix} i_{L1} \\ i_{L2} \\ u_{C1} \\ u_{C2} \end{pmatrix} + \begin{bmatrix} \frac{1}{L_1} \\ \frac{1}{L_2} \\ \frac{1}{RC_1} \\ \frac{1}{RC_2} \end{bmatrix} (u_1), \quad (13)$$

$$\frac{d}{dt} \begin{pmatrix} i_{L1} \\ i_{L2} \\ u_{C1} \\ u_{C2} \end{pmatrix} = \begin{bmatrix} 0 & 0 & -\frac{1}{L_1} & 0 \\ 0 & 0 & 0 & -\frac{1}{L_2} \\ \frac{1}{C_1} & 0 & -\frac{1}{RC_1} & -\frac{1}{RC_1} \\ 0 & \frac{1}{C_2} & -\frac{1}{RC_2} & -\frac{1}{RC_2} \end{bmatrix} \begin{pmatrix} i_{L1} \\ i_{L2} \\ u_{C1} \\ u_{C2} \end{pmatrix} + \begin{bmatrix} \frac{1}{L_1} \\ \frac{1}{L_2} \\ \frac{1}{RC_1} \\ \frac{1}{RC_2} \end{bmatrix} (u_1). \quad (14)$$

When the switching period is small compared to the time constants of the converter, one can write (13) with the duty cycle and (14) with one minus the duty cycle leading to

$$\frac{d}{dt} \begin{pmatrix} i_{L1} \\ i_{L2} \\ u_{C1} \\ u_{C2} \end{pmatrix} = \begin{bmatrix} 0 & 0 & \frac{d_1-1}{L_1} & 0 \\ 0 & 0 & 0 & \frac{d_2-1}{L_2} \\ \frac{1-d_1}{C_1} & 0 & -\frac{1}{RC_1} & -\frac{1}{RC_1} \\ 0 & \frac{1-d_2}{C_2} & -\frac{1}{RC_2} & -\frac{1}{RC_2} \end{bmatrix} \begin{pmatrix} i_{L1} \\ i_{L2} \\ u_{C1} \\ u_{C2} \end{pmatrix} + \begin{bmatrix} \frac{1}{L_1} \\ \frac{1}{L_2} \\ \frac{1}{RC_1} \\ \frac{1}{RC_2} \end{bmatrix} (u_1). \quad (15)$$

This model is nonlinear. To derive transfer functions and to construct Bode plots one has to linearize this matrix equation. This can be done by the perturbation method. The variables are written as combinations of the operating point value (written by capital letters with a zero in the index) and the perturbation of the operating point (written by small letters and a roof on top). For the operating point one gets the equations,

$$(D_{10} - 1)U_{C1} + U_{10} = 0, \quad (16)$$

$$(D_{20} - 1)U_{C1} + U_{10} = 0, \quad (17)$$

$$(1 - D_{10})I_{L10} - \frac{U_{C10}}{R} - \frac{U_{C20}}{R} + \frac{U_{10}}{R} = 0, \quad (18)$$

$$(1 - D_{20})I_{L10} - \frac{I_{LOAD}}{R} = 0. \quad (19)$$

It is easy to see that the results for the operating point values are equal to the results derived from inspecting the circuit in paragraph 2. The small signal model can be written according to,

$$\frac{d}{dt} \begin{pmatrix} \hat{i}_{L1} \\ \hat{i}_{L2} \\ \hat{u}_{C1} \\ \hat{u}_{C2} \end{pmatrix} = \begin{bmatrix} 0 & 0 & \frac{D_{10}-1}{L_1} & 0 \\ 0 & 0 & 0 & \frac{D_{20}-1}{L_2} \\ \frac{1-D_{10}}{C_1} & 0 & -\frac{1}{RC_1} & -\frac{1}{RC_1} \\ 0 & \frac{1-D_{20}}{C_2} & -\frac{1}{RC_2} & -\frac{1}{RC_2} \end{bmatrix} \begin{pmatrix} \hat{i}_{L1} \\ \hat{i}_{L2} \\ \hat{u}_{C1} \\ \hat{u}_{C2} \end{pmatrix} + \begin{bmatrix} \frac{1}{L_1} & \frac{U_{C10}}{L_1} & 0 \\ \frac{1}{L_2} & 0 & \frac{U_{C20}}{L_2} \\ \frac{1}{RC_1} & -\frac{I_{L10}}{C_1} & 0 \\ \frac{1}{RC_2} & 0 & -\frac{I_{L20}}{C_2} \end{bmatrix} \begin{pmatrix} \hat{u}_1 \\ \hat{d}_1 \\ \hat{d}_2 \end{pmatrix}. \quad (20)$$

With abbreviations for the elements of the state matrix and the input matrix,

$$\frac{d}{dt} \begin{pmatrix} \hat{i}_{L1} \\ \hat{i}_{L2} \\ \hat{u}_{C1} \\ \hat{u}_{C2} \end{pmatrix} = \begin{bmatrix} 0 & 0 & A_{13} & 0 \\ 0 & 0 & 0 & A_{24} \\ A_{31} & 0 & A_{33} & A_{34} \\ 0 & A_{42} & A_{43} & A_{44} \end{bmatrix} \begin{pmatrix} \hat{i}_{L1} \\ \hat{i}_{L2} \\ \hat{u}_{C1} \\ \hat{u}_{C2} \end{pmatrix} + \begin{bmatrix} B_{11} & B_{12} & 0 \\ B_{21} & 0 & B_{23} \\ B_{31} & B_{32} & 0 \\ B_{41} & 0 & B_{43} \end{bmatrix} \begin{pmatrix} \hat{u}_1 \\ \hat{d}_1 \\ \hat{d}_2 \end{pmatrix} \quad (21)$$

and using the Laplace transformation,

$$\begin{bmatrix} s & 0 & -A_{13} & 0 \\ 0 & s & 0 & -A_{24} \\ -A_{31} & 0 & s-A_{33} & -A_{34} \\ 0 & -A_{42} & -A_{43} & s-A_{44} \end{bmatrix} \begin{pmatrix} I_{L1}(s) \\ I_{L2}(s) \\ U_{C1}(s) \\ U_{C2}(s) \end{pmatrix} = \begin{bmatrix} B_{11} & B_{12} & 0 \\ B_{21} & 0 & B_{23} \\ B_{31} & B_{32} & 0 \\ B_{41} & 0 & B_{43} \end{bmatrix} \begin{pmatrix} U_1(s) \\ D_1(s) \\ D_2(s) \end{pmatrix} \quad (22)$$

one gets the transfer function between the output voltage and the duty cycles,

$$\frac{U_{C1}(s)}{D_1(s)} = \frac{s^3 B_{32} + s^2 (-A_{44} B_{32} + A_{31} B_{12}) + s (-A_{24} A_{42} B_{32} - A_{31} A_{44} B_{12}) - A_{24} A_{31} A_{42} B_{12}}{s^4 + s^3 (-A_{33} - A_{44}) + s^2 (-A_{24} A_{42} - A_{34} A_{43} - A_{13} A_{31} + A_{33} A_{44}) + s (+A_{24} A_{33} A_{42} + A_{13} A_{31} A_{44}) + A_{13} A_{24} A_{31} A_{42}}, \quad (23)$$

$$\frac{U_{C1}(s)}{D_2(s)} = \frac{s (A_{34} B_{43} s + A_{34} A_{42} B_{23})}{s^4 + s^3 (-A_{33} - A_{44}) + s^2 (-A_{24} A_{42} - A_{34} A_{43} - A_{13} A_{31} + A_{33} A_{44}) + s (+A_{24} A_{33} A_{42} + A_{13} A_{31} A_{44}) + A_{13} A_{24} A_{31} A_{42}}. \quad (24)$$

This model is useful when the parameters of the converter stages differ. It should not be used when the values of the components are equal in both boost parts of the converter.

When the converter is built symmetrically, it is easier to use a second order model for one converter stage and multiply the result of the output voltage by two and subtract the input voltage. In this case, one gets the simple model from Eqs. (8-12) according to,

$$\frac{d}{dt} \begin{pmatrix} \hat{i}_L \\ \hat{u}_C \end{pmatrix} = \begin{bmatrix} 0 & \frac{D_0-1}{L} \\ \frac{1-D_0}{C} & -\frac{2}{RC} \end{bmatrix} \begin{pmatrix} \hat{i}_L \\ \hat{u}_C \end{pmatrix} + \begin{bmatrix} \frac{1}{L} & \frac{U_{C0}}{L} \\ \frac{1}{RC} & -\frac{I_{L0}}{C} \end{bmatrix} \begin{pmatrix} \hat{u}_1 \\ \hat{d} \end{pmatrix}. \quad (25)$$

The transfer function can be calculated to,

$$\frac{U_C(s)}{D(s)} = \frac{sB_{22} + A_{21}B_{12}}{s^2 - A_{22}s - A_{12}A_{21}} = \frac{-1.7212e4 \cdot s + 1.5465e9}{s^2 + s \cdot 4.8485e2 + 2.8920e7} \quad (26)$$

where the working point parameters are $D_0=0.33$, $U_{10}=24$ V, $R=12.5$ Ω , $U_{20}=47.6$ V, $U_{C0}=35.8$ V, $I_{LOAD}=3.8$ A, $I_{L0}=5.68$ A, calculated with ideal working point equations. Fig. 6 shows the Bode plot and the step response for one converter part. The transfer function describes a non-phase minimum system. The zero is on the right side of the complex plane. The zero can be calculated according to,

$$s_Z = -\frac{A_{21}B_{12}}{B_{22}} = -\frac{\frac{1-D_0}{C} \frac{U_{C0}}{L}}{-\frac{I_{L0}}{C}} = \frac{U_{C0}}{I_{L0}} \frac{1-D_0}{L} = 8.9849e4 \quad (27)$$

with a zero frequency at 14.3 kHz.

The larger the inductor value, the greater the influence of the zero. To reduce the influence of the zero the frequency should be high, so a small inductor is enough. The position of the poles can be found at,

$$s_{P1,P2} = A_{22} \pm \sqrt{A_{22}^2 + A_{12}A_{21}} \quad (28)$$

The poles are at $-2.4243e2 + j5.3723e3$ and the pole frequency is at 855 Hz.

The DC-gain is 35 dB 56.2, and changing the duty cycle by 0.01 changes the capacitor voltage by 56.2 mV. The damping is caused by

$$\delta = A_{22} = -\frac{2}{RC} \quad (29)$$

A small load resistor (high load) damps the system, also a small capacitor. The Bode plot and the step response are shown in Fig. 5.

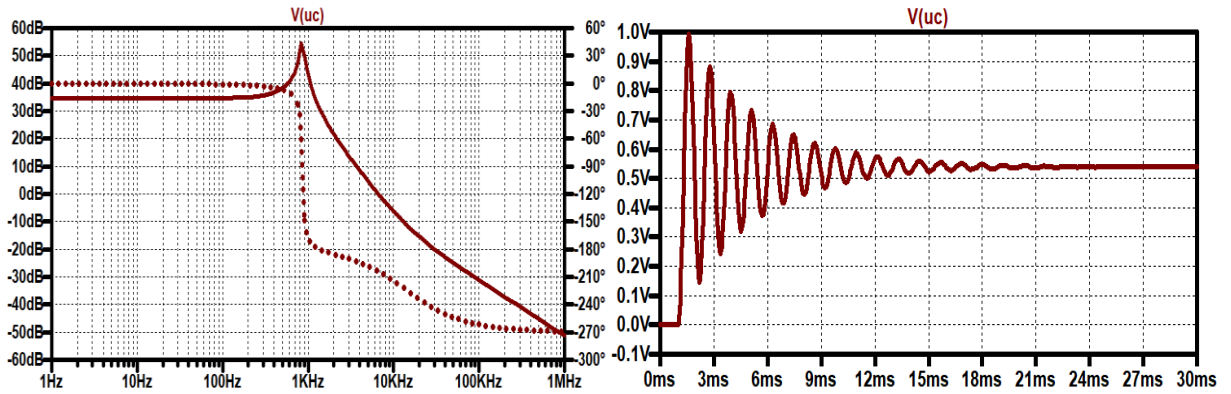


Figure 6. Bode plot (solid line: gain response, dotted line: phase response), step response.

Fig. 7 shows the start-up of the converter (inrush omitted, the converter starts with already charged capacitors) and the transients caused by changes of the duty cycle. The steps are small, six or three percent up and down. To avoid large current amplitudes during the transient, one must use a ramp to change the duty cycle instead of steps.

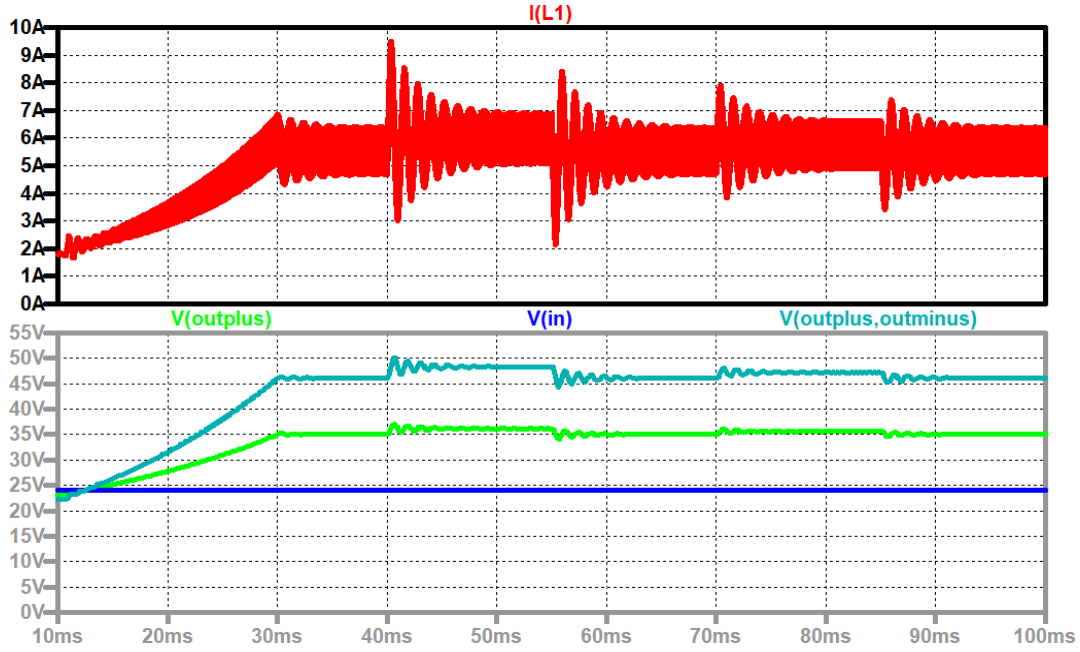


Figure 7. Floating double Boost converter, duty cycle steps, up to down: current through L1 (red); output voltage (turquoise), voltage at the output of the first converter stage (green), input voltage (blue).

4. INRUSH CURRENT

The inrush depends on the resonances of the two Boost converters. The peak current depends on the slope of the input voltage, when it is turned on. For a step (and omitting the converter losses and the load) the current is a positive half-wave (when the current reaches zero, the diode turns off). The inrush current can be calculated and the idealized input peak current for the model parameters (for a single stage) and the time for the peak can be found by,

$$i = 2\sqrt{\frac{C}{L}}U_1 \sin\left(\sqrt{\frac{1}{LC}}t\right), \quad (30)$$

$$\hat{I}_1 = 2\sqrt{\frac{C}{L}}U_1 = 127 \text{ A}, \quad (31)$$

And,

$$T_1 = \pi\sqrt{CL} = 391 \mu\text{s}, \quad (32)$$

respectively. The peak current through the coils is 63.6 A. One must keep in mind that the coils will saturate, the value of the coils decreases and the peak current is even higher. Fig. 8 shows the idealized inrush current, the current through one coil, the input voltage, the current across the upper capacitor, and the output voltage. The output voltage is negative at the beginning because the capacitors are discharged when the input source is connected.

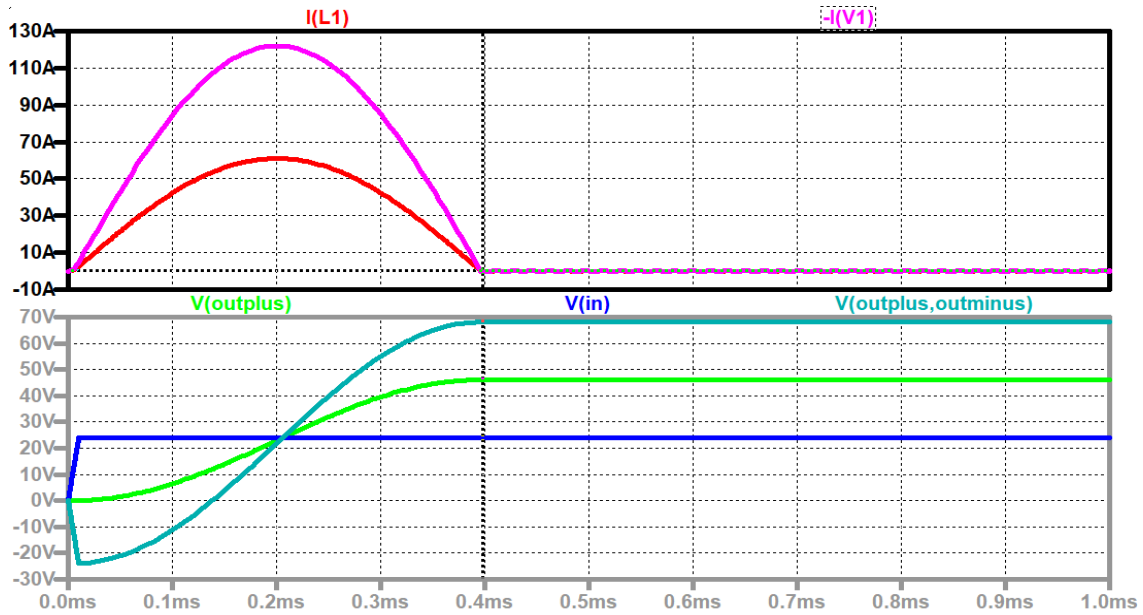


Figure 8. Idealized inrush, up to down: input current (violet), current through L1 (red); output voltage (turquoise), voltage across C1 (green), input voltage (blue).

With an additional input transistor S_{IN} which starts with a duty cycle from zero and increases to one by a ramp function, the current into the converter can be reduced and controlled. This additional transistor can also be used as a fuse to turn off the converter very fast in the case of a short-circuit, open-circuit, overcurrent or overheat. Between the drain of the transistor S_{IN} and the anode of the additional diode D_{IN} , an input capacitor has to be connected. Fig. 9 shows the circuit diagram of the converter with the additional input stage.

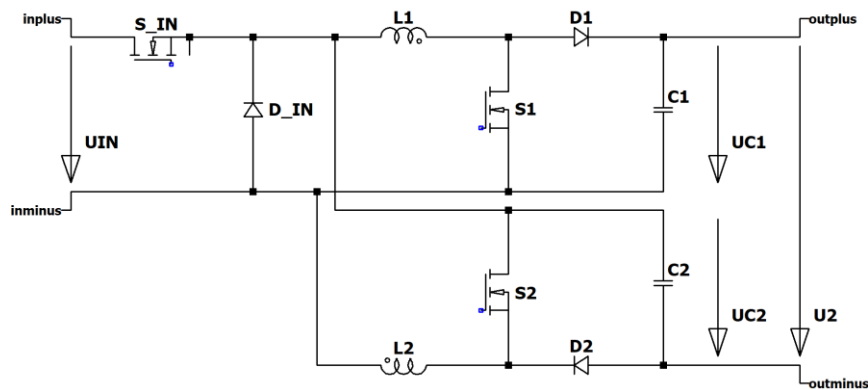


Figure 9. Converter with additional input stage

In Figs. 10 and 11 the current through one coil, the output voltage, the voltages across the two capacitors, and the input voltage during such a turn on are shown. When S_{IN} is turned on, the positive input voltage U_{IN} is across the coils, and when S_{IN} is turned off, the current free-wheels through D_{IN} . When the converter is working, S_{IN} must be on all the time. When the pre-stage must work as fuse S_{IN} must be off.

Fig. 10 shows the turn-on with no load, and Fig. 11 with load. The current through L1 is depicted, the current through the other coil looks the same, and the input current is therefore double as large. The output voltage, the voltages across the capacitors, and the input voltage are also shown in these figures.

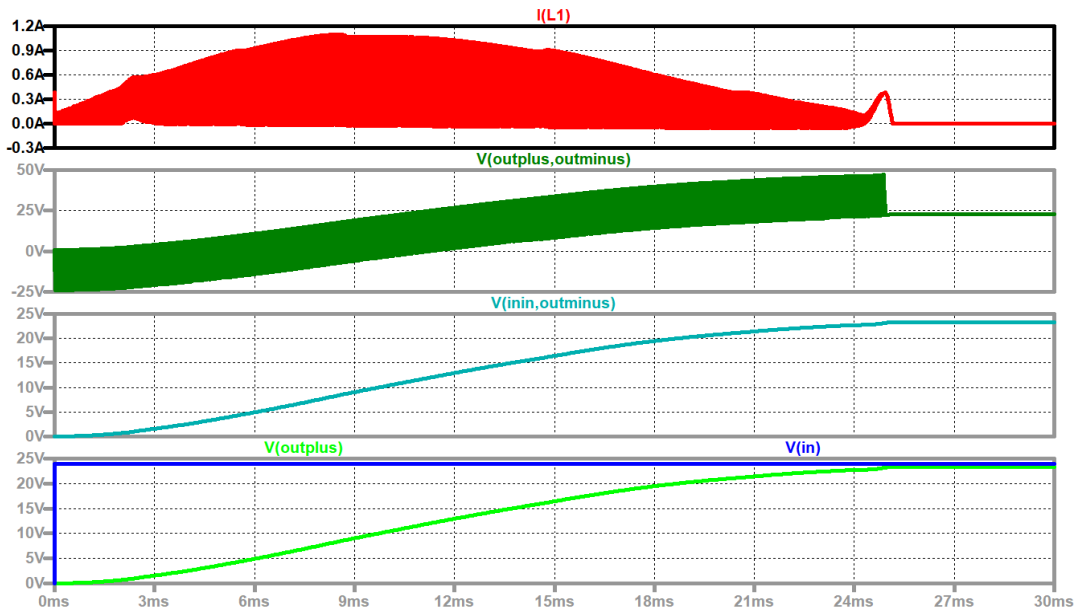


Figure 10. Floating double Boost with additional inrush current reduction (no load), up to down: current through the first coil (red); output voltage (dark green); voltage across second capacitor(turquoise); input voltage (blue), voltage across the first capacitor (green).

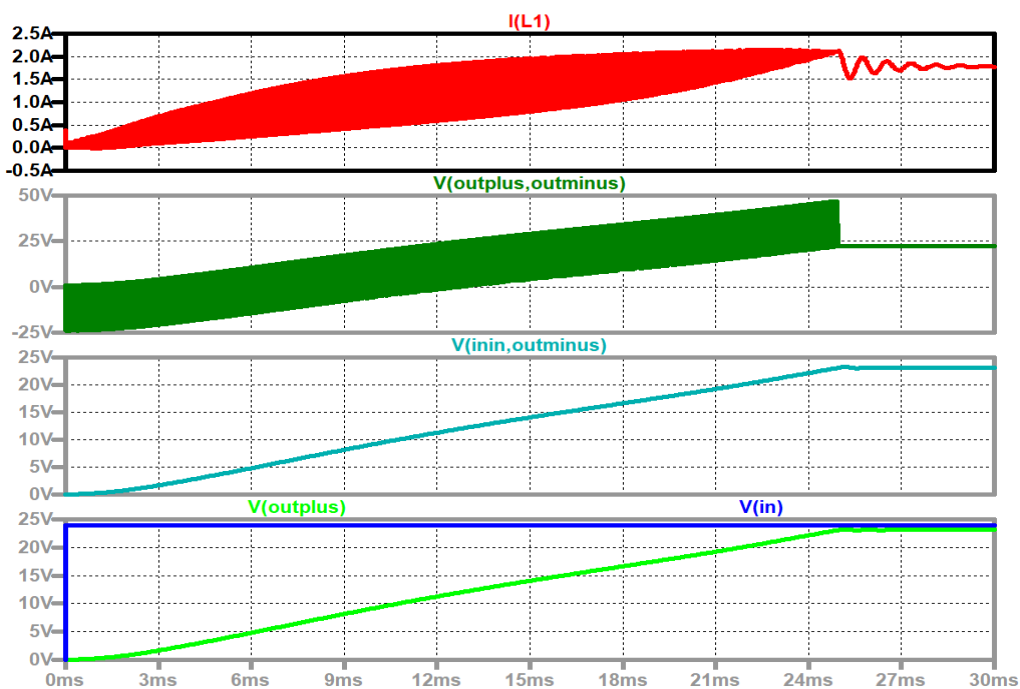


Figure 11. Floating double Boost with additional inrush current reduction (with load), up to down: current through the first coil (red); output voltage (dark green); voltage across the second capacitor(turquoise); input voltage (blue), voltage across first capacitor (green).

5. INFLUENCE OF THE PARASITIC CAPACITORS ON THE FLOATING SIDE

An important aspect of floating converters are capacitive currents to the ground. There are two possibilities to ground the system: at the output or at the input side.

5.1. Floating Input - Grounded Output

When the load is connected to ground, the output side of the converter has to be fixed to ground. The input source is floating. The output is connected to ground. The mean voltage across the two connectors of the input voltage source is now shifted in reference to the ground according to,

$$U_{IN_plus} = (+U_{C2}), \quad (33)$$

$$U_{IN_minus} = (-U_1 + U_{C2}). \quad (34)$$

With large output capacitors (C_1, C_2) the voltages are nearly constant across these capacitors. With a stable input voltage, the input voltage is only shifted to the ground and the capacitive displacement currents or the leakage currents through C_{plus} and C_{minus} from the input source are small and can be neglected as shown in Fig. 12.

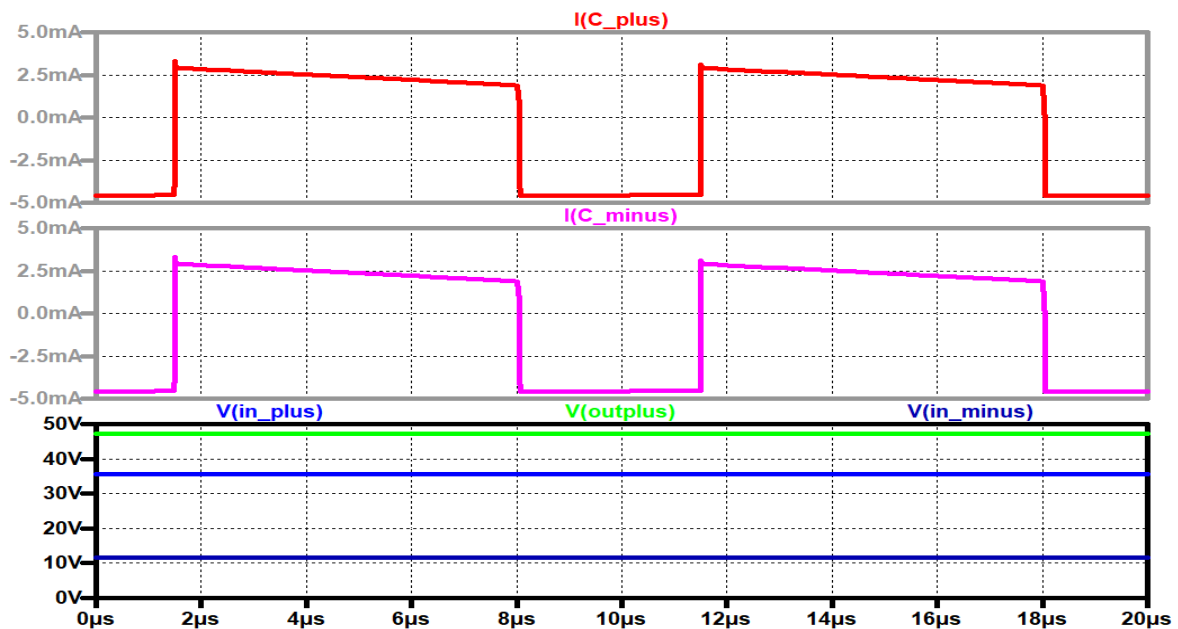


Figure 12. Current from the positive input terminal to ground (red), current from the negative input terminal to ground (violet), output voltage (green), voltage between the positive input terminal to ground (blue), voltage between the negative input terminal to ground (dark blue).

For a more realistic result one has to include the parasitic series resistors of the output capacitors (C_1, C_2). At every switching event the current through the output capacitors changes its direction. The simulation is done with $30\text{ m}\Omega$ series resistor of the output capacitors (Fig. 13).

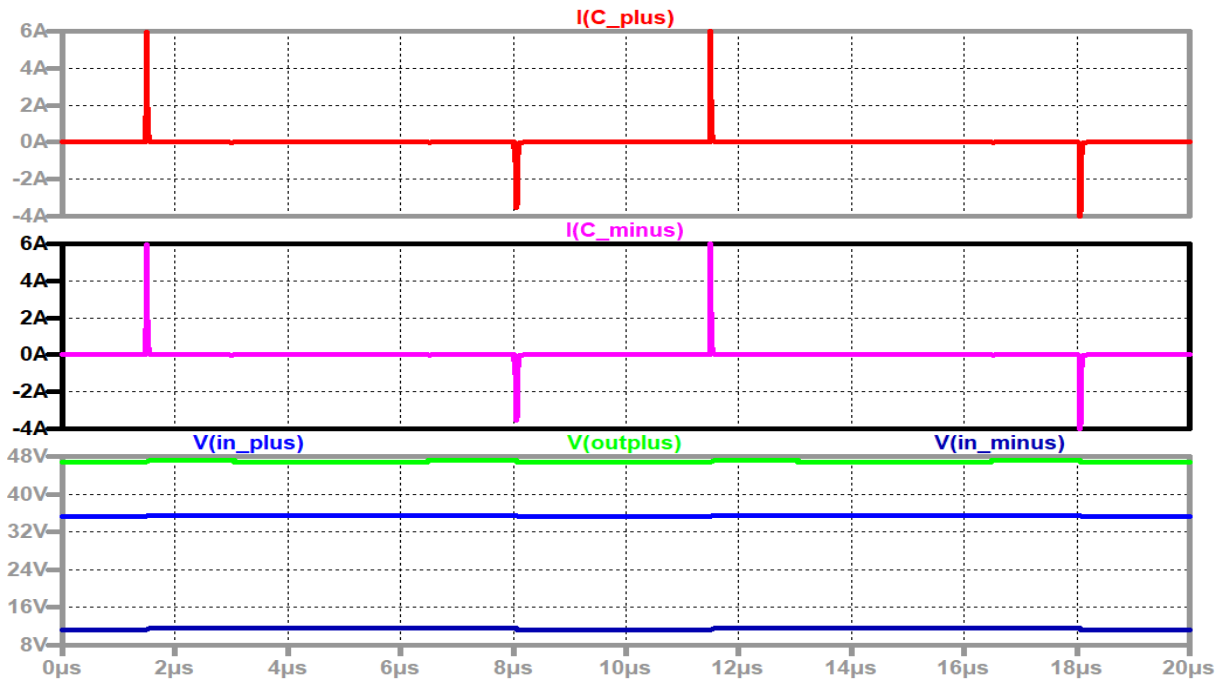


Figure 13. Current from the positive input terminal to ground (red) through C_{plus} , current from the negative input terminal to ground (violet) through C_{minus} , output voltage (green), voltage between the positive input terminal to ground (blue), voltage between the negative input terminal to ground (dark blue)

The simulation circuit is depicted in Fig. 14.

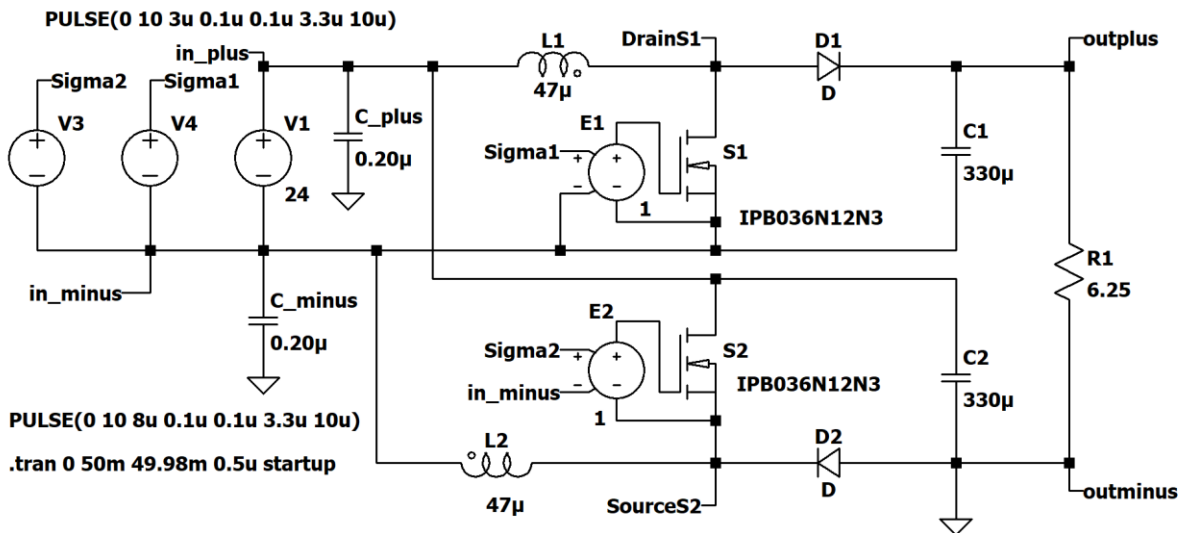


Figure 14. Simulation circuit.

The change of the direction of the current through the floating output capacitor $C1$ has no effect on the leakage currents. The change of the direction of the current produces fast voltage steps across the parasitic resistors of the output capacitors and these voltage steps produce displacement currents through the capacitors (C_{plus} , C_{minus}) between the input voltage source and ground.

Fig. 15 shows the current ripple of the current through the coils $L2$ $L1$, the voltage step across $C1$ and the voltage step across $C2$, the current through the floating output capacitor, the current through the grounded output capacitor, current through the leakage capacitors C_{plus} and the leakage capacitor C_{minus} , the output voltage, the voltage between the positive input terminal to ground, the voltage between the negative input terminal to ground, and the control signal of $S1$ and $S2$.

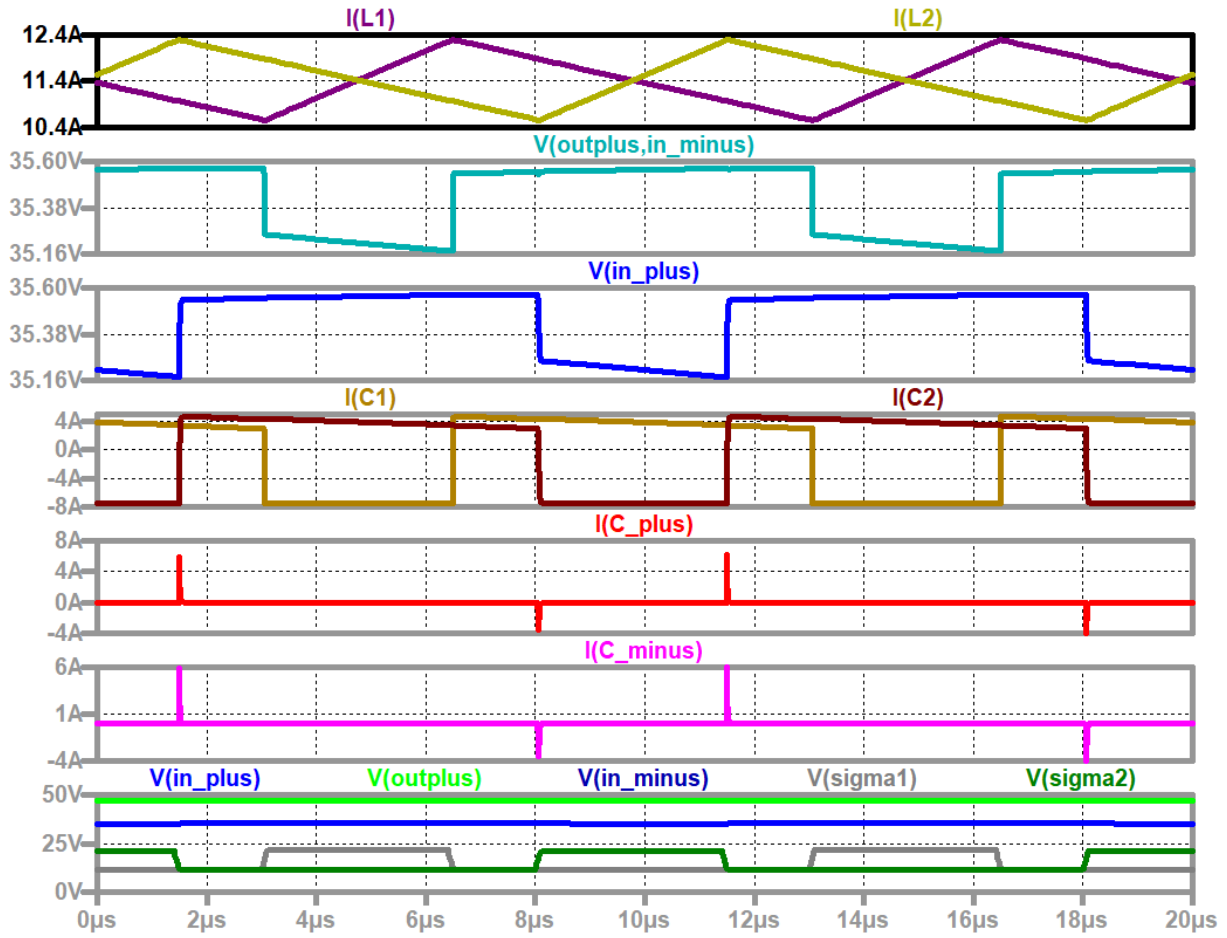


Figure 15. Current ripple of the current through L2 (light brown), current ripple of the current through L1 (dark violet); voltage step across C1 (turquoise); voltage step across C2 (blue); current through the floating output capacitor (brown), current through the grounded output capacitor (black); current through the leakage capacitor C_{plus} (red); current through the leakage capacitor C_{minus} (violet); output voltage (green), voltage between the positive input terminal to ground (blue), voltage between the negative input terminal to ground (dark blue), control signal of S1 (grey, referred to ground), control signal of S2 (dark green, referred to ground)

5.2. Floating Output - Grounded Input

The second possibility to ground the system is on the input side. For security reasons it can be useful to connect one pole of the input source to ground. We test the system again and consider the parasitic resistor (30 mΩ) of the output capacitors (C1, C2). In Fig. 16 the current ripple of the current through L2, the current ripple of the current through L1, the voltage step across C1, the voltage step across C2 (blue), the current through the floating output capacitor, the current through the grounded output capacitor, the current through the leakage capacitor C_{minus}, the current through the leakage capacitor C_{plus}, the output voltage, the voltage between the negative input terminal to ground, the control signal of S1, and the control signal of S2.

The parasitic resistors of the output capacitors (C1, C2) cause, in combination with the change of the direction of the current, a capacitive current flowing from the output to ground. Therefore, excellent capacitors with low series resistor should be used.

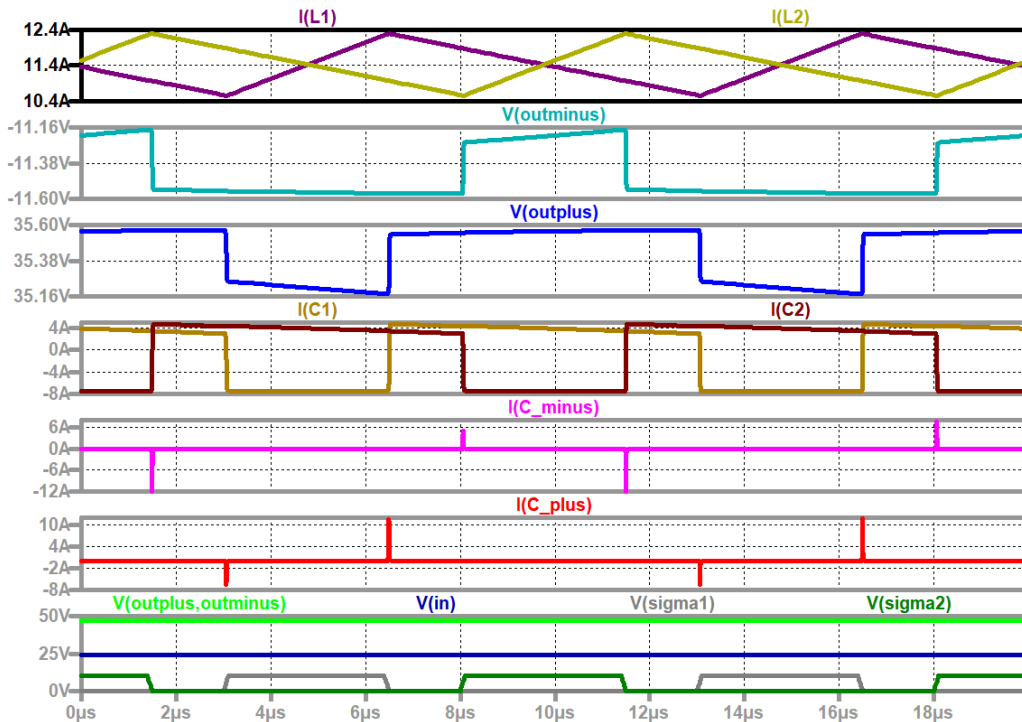


Figure 16 . Current ripple of the current through L2 (light brown), current ripple of the current through L1 (dark violet); voltage step across C1 (turquoise); voltage step across C2 (blue); current through the floating output capacitor (brown), current through the grounded output capacitor (black); current through the leakage capacitor C_minus (violet), current through the leakage capacitor C_plus (red); output voltage (green), voltage between the negative input terminal to ground (dark blue), control signal of S1 (grey, referred to ground), control signal of S2 (dark green, referred to ground)

6. FURTHER MODIFICATIONS

6.1. Modified Floating Two Stage Double Boost Converter

A second way to avoid the inrush current when a stable supply has to be connected is to modify the circuit by changing the position of the capacitors as shown in Fig. 17, thus avoiding the inrush completely. The bulk capacitors (C1, C2) of the converter are now connected not at the output of the two stages but between the output and the input. This modification is significant, when the input voltage is a stiff one because changes of the input voltage immediately effect the output voltage. Fig. 18 shows the input voltage, the output voltage and the current through the source. When the input voltage is applied, the output voltage immediately reaches the input voltage, and the input current reaches the value which is necessary to supply the load. Only a small ringing occurs.

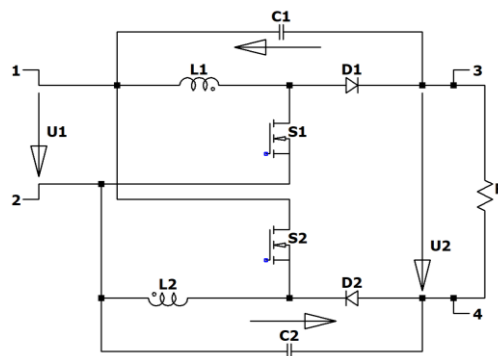


Figure 17. Modified two stage floating boost converter.

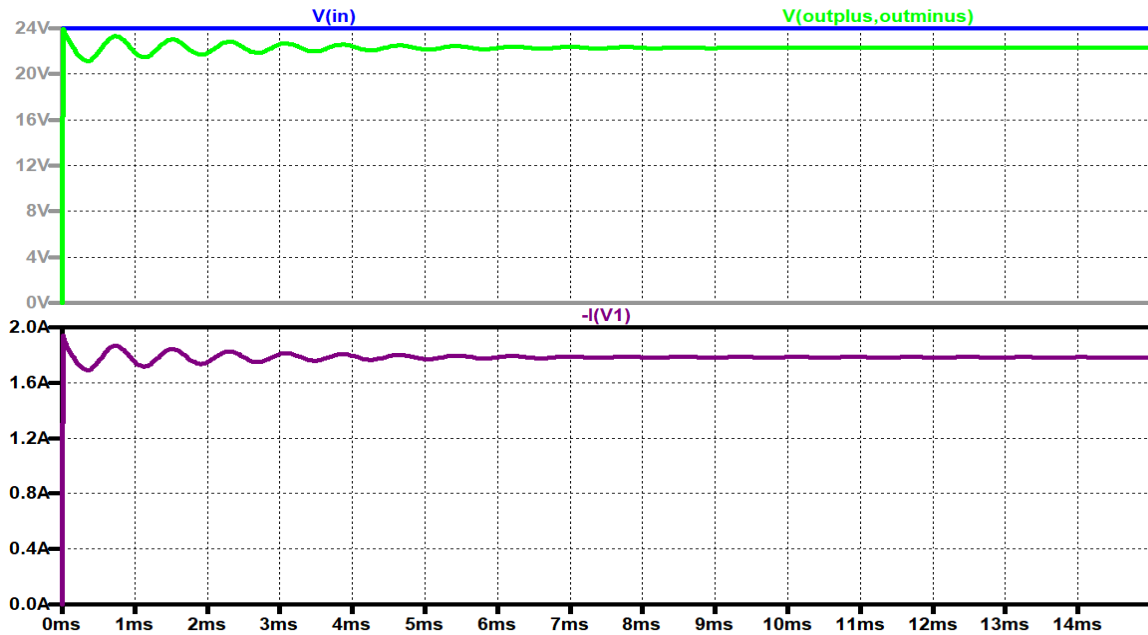


Figure 18. Modified floating two stage Boost converter: input voltage (blue), output voltage (green); input current (dark violet)

6.2. Reduction of the Forward Losses

To reduce the onward losses, the diodes are replaced by electronic switches (S3, S4) which have lower conduction losses than the diodes. Fig. 19 shows the circuit diagram. Besides the active switches, two additional floating drivers are necessary which increase the costs of the system. Correct control of these switches is also necessary. They must be turned on after the main switches (S1, S2) turn off, and off before the main switches turn on again. The antiparallel diodes (D3, D4) of the additional active switches (S3, S4) can turn on in the intermediate time.

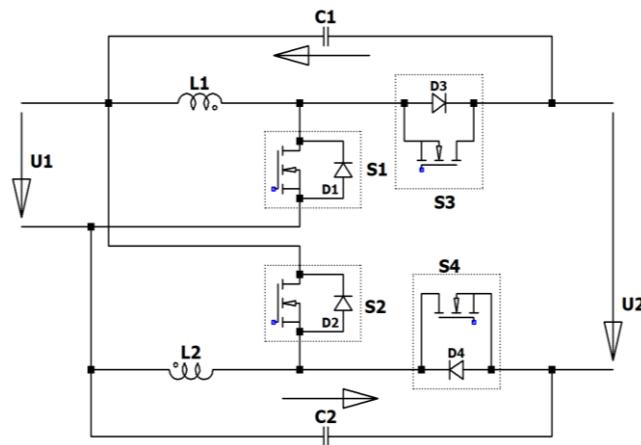


Figure 19. Modified floating two stage boost converter with active switches instead of the diodes.

7. EXPERIMENT

A small converter laboratory model was built with 47 μH coils and capacitors with 330 μF . The switching frequency was chosen to 100 kHz. ACPL-P343 floating drivers were used to control the active switches.

Fig. 20 shows the voltages across the electronic switches and the current through the coils in the continuous mode.

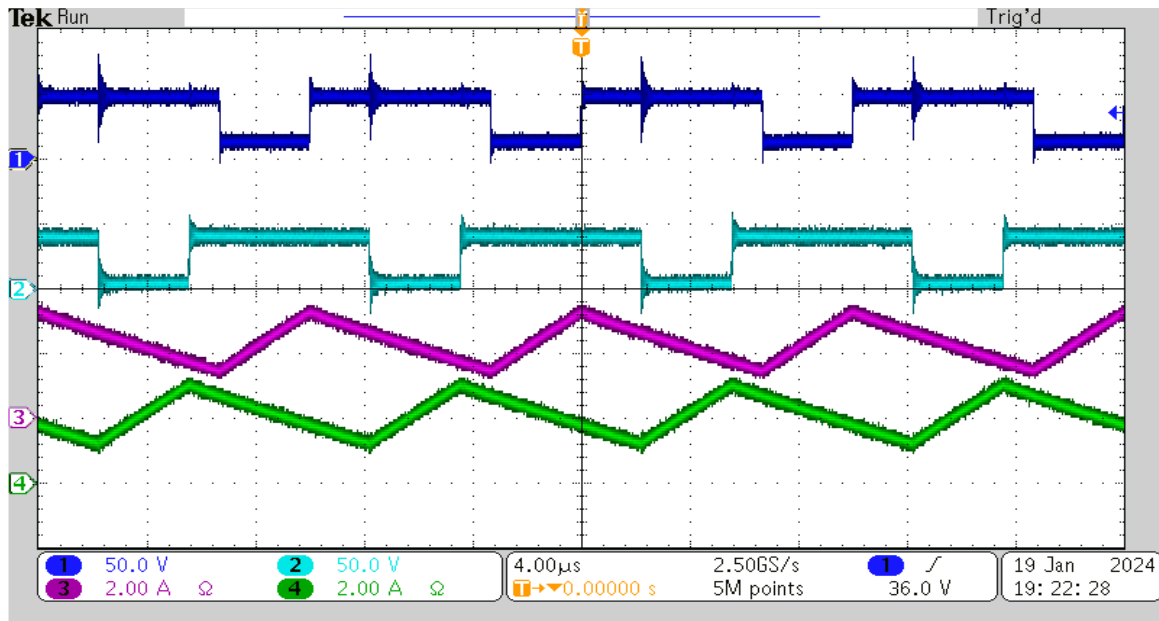


Figure 20. Continuous mode, up to down: voltage across switch S1 (blue), voltage across switch S2 (turquoise), current through L1 (violet), current through L2 (green).

Fig. 21 shows the voltages across the electronic switches and the currents through the coils in the discontinuous mode. The ringing is caused by the parasitic capacitors of the diode and the switch and is typical for discontinuous operation.

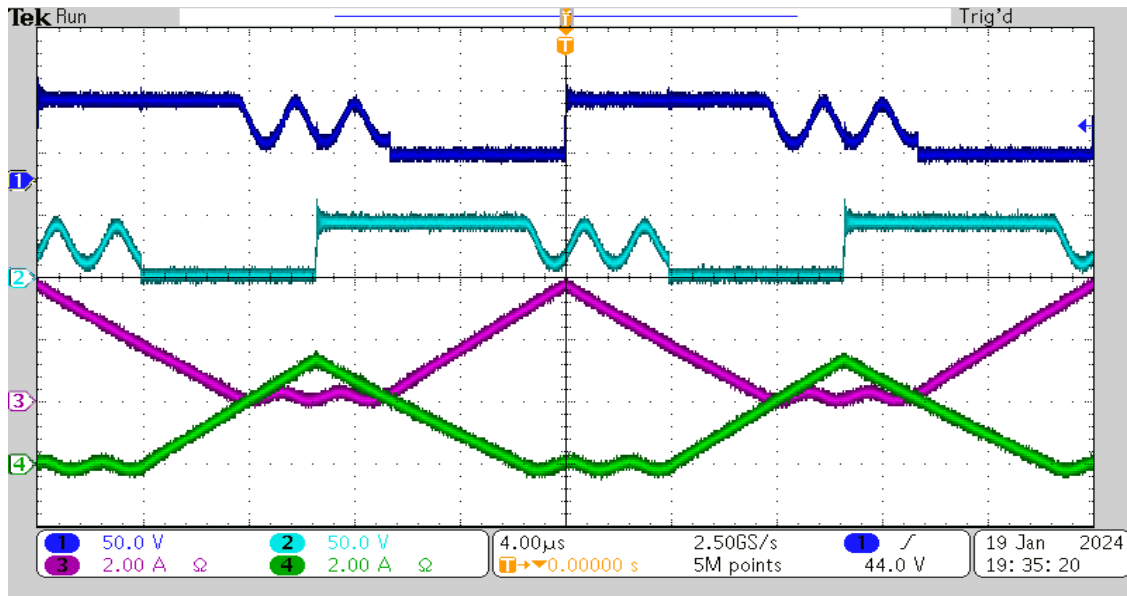


Figure 21. Discontinuous mode, up to down: voltage across switch S1 (blue), voltage across switch S2 (turquoise), current through L1 (violet), current through L2 (green).

Fig. 22 shows the voltages across the electronic switches and the current through the coils near the border between continuous and discontinuous modes. One can see the decreasing voltage across the switches immediately before turn-on.

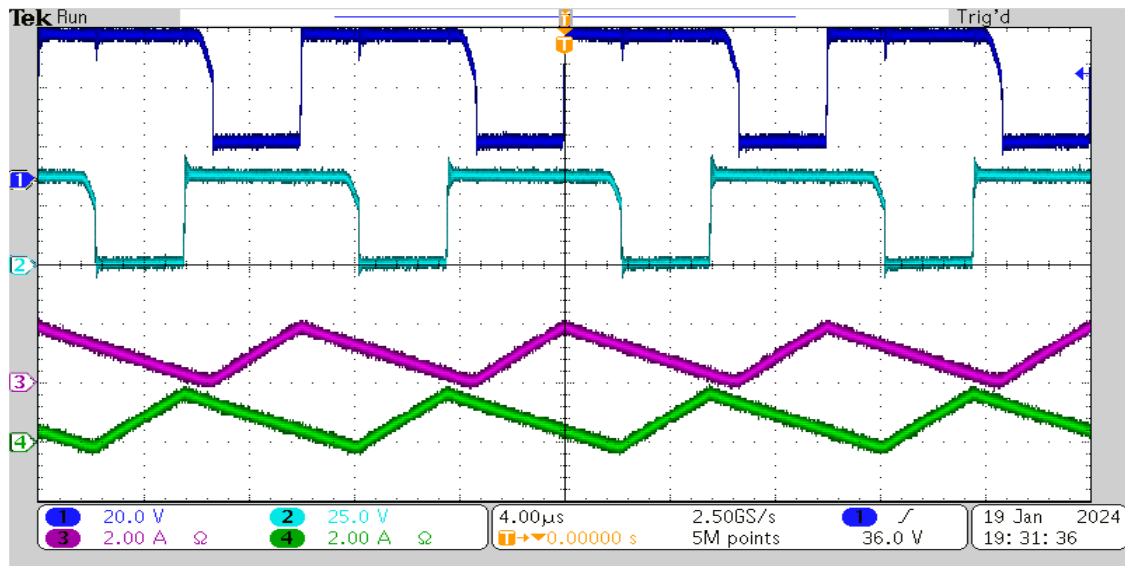


Figure 22. Boundary mode, up to down: voltage across switch S1 (blue), voltage across switch S2 (turquoise), current through L1 (violet), current through L2 (green)

8. CONCLUSION

The floating double boost converter has some interesting features:

- Voltage transformation ratio $(1+d)/(1-d)$,
- The processed power is parted into two converters, so the losses and the produced heat are better distributed,
- It can be easily combined with an additional two switch-diode pre-stage to avoid the inrush and which can be used as a fuse,
- Both converters should be controlled by the same duty cycle, the system to be controlled can so be simplified to a second order system,
- The ripple of the input is reduced compared to a single Boost converter.
- A small modification of the position of the bulk capacitors also avoids the inrush current.
- Replacing the diodes by active switches can reduce the conduction losses.

The converter is useful for solar and fuel-cell applications.

REFERENCES

- [1] Mohan N, Undeland T, Robbins W. *Power Electronics, Converters, Applications and Design*. 3rd ed. New York, NY: John Wiley & Sons; 2003.
- [2] Zach F. *Leistungselektronik*. 6th ed. Frankfurt, Germany: Springer; 2022.
- [3] Rozanov Y, Ryvkin S, Chaplygin E, Voronin P. *Power Electronics Basics*. Boca Raton, FL: CRC Press; 2016.
- [4] Forouzesh M, Siwakoti YP, Gorji SA, Blaabjerg F, Lehman B. Step-Up DC–DC Converters: A Comprehensive Review of Voltage-Boosting Techniques, Topologies, and Applications. *IEEE Trans Power Electron.* 2017;32(12):9143-9178. doi:10.1109/TPEL.2017.2652318.
- [5] Williams BW. Generation and Analysis of Canonical Switching Cell DC-to-DC Converters. *IEEE Trans Ind Electron.* 2014;61(1):329-346. doi:10.1109/TIE.2013.2240633.
- [6] Cuk S. General topological properties of switching structures. In: *IEEE Power Electronics Specialists Conference*; 1979; San Diego, CA, USA. p. 109-130.

- [7] Simões MG, Lute CL, Alsaleem AN, Brandao DI, Pomilio JA. Bidirectional floating interleaved buck-boost DC-DC converter applied to residential PV power systems. In: *2015 Clemson University Power Systems Conference (PSC)*; 2015; Clemson, SC, USA. p. 1-8. doi:10.1109/PSC.2015.7101675.
- [8] Coutellier D, Agelidis VG, Choi S. Experimental verification of floating-output interleaved-input DC-DC high-gain transformer-less converter topologies. In: *2008 IEEE Power Electronics Specialists Conference*; 2008; Rhodes, Greece. p. 562-568. doi:10.1109/PESC.2008.4591989.
- [9] Kabalo M, Blunier B, Bouquain D, Miraoui A. Comparison analysis of high voltage ratio low input current ripple floating interleaving boost converters for fuel cell applications. In: *2011 IEEE Vehicle Power and Propulsion Conference*; 2011; Chicago, IL, USA. p. 1-6. doi:10.1109/VPPC.2011.6043101.
- [10] Miranda M, Banakar P, Gunnal G, Kiran Kumar V. Robust Voltage Control of Improved Floating Interleaved Boost Converter for Photovoltaic Systems. In: *ICCCS 2020 5th International Conference on Computing, Communication and Security*; 2020; Patna, India. p. 1-5. doi:10.1109/ICCCS49678.2020.9276866.
- [11] Kabalo M, Paire D, Blunier B, Bouquain DM, Simoes G, Miraoui A. Experimental Validation of High-Voltage-Ratio Low-Input-Current-Ripple Converters for Hybrid Fuel Cell Supercapacitor Systems. *IEEE Trans Veh Technol.* 2012;61(8):3430-3440. doi:10.1109/TVT.2012.2208132.
- [12] Xu L, et al. Extended State Observer-Based Sliding-Mode Control for Floating Interleaved Boost Converters. In: *IECON 2018 - 44th Annual Conference of the IEEE Industrial Electronics Society*; 2018; Washington, DC, USA. p. 5283-5289. doi:10.1109/IECON.2018.8591138.
- [13] Huangfu Y, Guo L, Ma R, Gao F. An Advanced Robust Noise Suppression Control of Bidirectional DC-DC Converter for Fuel Cell Electric Vehicle. *IEEE Trans Transp Electrifi.* 2019;5(4):1268-1278. doi:10.1109/TTE.2019.2943895.
- [14] Li Q, et al. An Improved Floating Interleaved Boost Converter with the Zero-Ripple Input Current for Fuel Cell Applications. *IEEE Trans Energy Convers.* 2019;34(4):2168-2179. doi:10.1109/TEC.2019.2936416.
- [15] Li Q, Huangfu Y, Zhao J, Zhuo S, Chen F. Controller design and fault tolerance analysis of 4-phase floating interleaved boost converter for fuel cell electric vehicles. In: *IECON 2017 - 43rd Annual Conference of the IEEE Industrial Electronics Society*; 2017; Beijing, China. p. 7753-7758. doi:10.1109/IECON.2017.8217359.
- [16] Lute CD, Simões MG, Brandao DI, Durra AA, Muyeen SM. Experimental evaluation of an interleaved boost topology optimized for peak power tracking control. In: *IECON 2014 - 40th Annual Conference of the IEEE Industrial Electronics Society*; 2014; Dallas, TX, USA. p. 2096-2102. doi:10.1109/IECON.2014.7048791.
- [17] Sartipizadeh H, Harirchi F, Babakmehr M, Dehghanian P. Robust Model Predictive Control of DC-DC Floating Interleaved Boost Converter with Multiple Uncertainties. *IEEE Trans Energy Convers.* 2021;36(2):1403-1412. doi:10.1109/TEC.2021.3058524.
- [18] Lin P, Jiang W, Wang J, Shi D, Zhang C, Wang P. Toward Large-Signal Stabilization of Floating Dual Boost Converter-Powered DC Microgrids Feeding Constant Power Loads. *IEEE J Emerg Sel Top Power Electron.* 2021;9(1):580-589. doi:10.1109/JESTPE.2019.2956097.
- [19] Lute M, Simões G, Brandao DI, Al Durra A, Muyeen SM. Development of a four phase floating interleaved boost converter for photovoltaic systems. In: *ECCE 2014 IEEE Energy Conversion Congress and Exposition*; 2014; Pittsburgh, PA, USA. p. 1895-1902. doi:10.1109/ECCE.2014.6953650.
- [20] Himmelstoss FA, Votzi HL. A Floating Double Buck-Boost Converter as Driver for a Permanent Exited DC Machine. In: *EDPE 2023 International Conference on Electrical Drives & Power Electronics*; 2023. p. 72-77. doi:10.1109/EDPE53134.2021.9604062.
- [21] Himmelstoss FA. Tristate Converters. *WSEAS Trans Power Syst.* 2023;18:259-269. doi:10.37394/232016.2023.18.27.
- [22] Corak I., & Cetin S., 8 MHz high efficient resonant sepic converter design for led driver of endoscopy systems”, *Journal of Polytechnic*, 2024;27(2): 461-468, DOI: 10.2339/politeknik.1118158.